Analysis of the Material Behavior of 3D Printed Laminates Via FFF

M. Somireddy [1] · C.V. Singh [2,3] · A. Czekanski [1]

Abstract

A comprehensive understanding of process–structure–property relationship of 3D printed parts is currently limited. In the present study, we investigate the influence of the mesostructure on the overall mechanical behavior of the parts synthesized via fused filament fabrication. In particular, characterization of anisotropic behavior is carefully studied by performing mechanical testing on the printed parts. The printed parts are treated as laminates and are characterized using laminate mechanics. Test coupons of thick layered and also thin layered unidirectional as well as bidirectional laminates are printed with polymeric material for tensile and bending tests. Test results revealed that the process parameters govern the mesostructure and therefore the material behavior of the parts. Mechanical behavior of the bidirectional printed laminates is studied in detail. The properties are significantly influenced by the layer thickness and layup order of the printed parts. Mechanical behavior of the printed parts can be characterized using laminate theory. The effect of lamina layup and layer thickness on the flexural properties of the laminates is significant. Furthermore, the first ply failure theory is employed for the finite element failure analysis of the printed parts. The results provide insights in the relationship between mesostructure–mechanical properties of the printed parts.

Nomenclature

L	Length of specimen
W	Width of specimen
T	Thickness of specimen
TL	Tab length
l	Span length of specimen
$\theta°$	Raster angle (Fiber angle, printing direction)
t	Layer(lamina) thickness of specimen (t_1 or t_2)
E_1	Young's Modulus of lamina in direction 1
E_2	Young's Modulus of lamina in direction 2
G_{12}	Shear modulus of lamina in plane 1–2
ν_{12}	Poisson's ratio
X_t	Longitudinal strength of lamina in tension
Y_t	Transverse strength of lamina in tension
S	Inplane shear strength of lamina
E_x	Young's modulus of laminate in direction x
U_t	Ultimate tensile strength of laminate
ε_t	Strain to failure of laminate
σ_{ply}	Principal stress of lamina
ε_{ply}	Elastic strain of lamina
E_x^f	Flexural stiffness of laminate in direction x
U_x^f	Flexural strength of laminate in direction x

✉ A. Czekanski
   alex.czekanski@lassonde.yorku.ca

1 Department of Mechanical Engineering, York University, Toronto, ON M3J 1P3, Canada

2 Department of Materials Science and Engineering, University of Toronto, Toronto, ON M5S 3E4, Canada

3 Department of Mechanical and Industrial Engineering, University of Toronto, Toronto, ON M5S 3G8, Canada

Introduction

Additive manufacturing (AM) techniques, or 3D printing, allow fabrication of any complex geometric three-dimensional parts through layer-by-layer deposition of material, while enabling rapid prototyping, minimal material wastage, efficient design of materials, and fabrication of functionally graded material parts [1]. Different multi directional preforms for composites can be designed and fabricated via AM techniques [2]. A primary concern related to these techniques is the inconsistency of the material properties of the printed part, as the material properties of the final printed part are not the same as those of the material used in the manufacturing of the part [3]. That means the anisotropy in the properties is introduced during the deposition of the material and it is because of a change in the mesostructure of the part while it is being printed. The composite materials used to print the parts also promote anisotropic behavior [4]. Further, the failure behavior of the printed parts

Fig. 1 3D printing of a part by layer upon layer deposition of the material via fused filament fabrication method
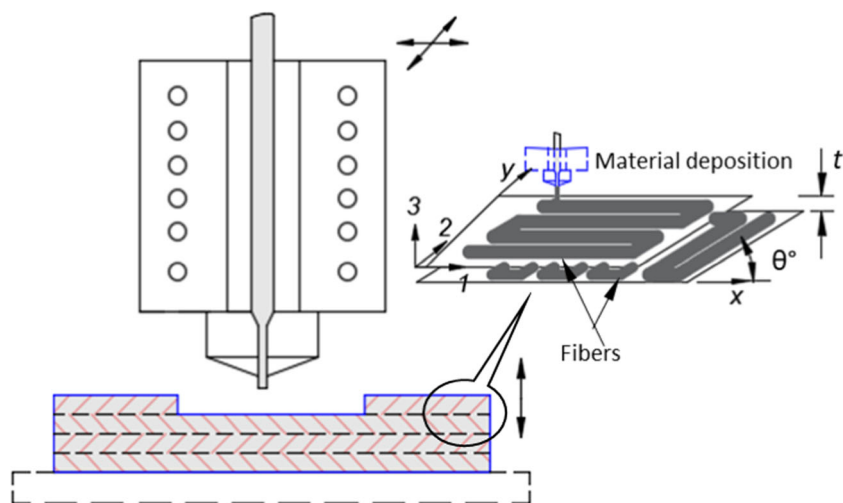
is not exhibited consistently because of the presence of anisotropy in the properties of materials. Moreover, no single failure mode is responsible for the ultimate failure of the part [5, 6]. The complex failure behavior and anisotropic properties of the final printed material complicate the design of the parts for 3D printing. Therefore, understanding the final material properties of the printed part and its failure behavior will allow for the effective design and analysis of the part for 3D printing.

A material extrusion AM technique, fused filament fabrication (FFF), printed parts are considered for the investigation in the present study. This process is also known as fused deposition modeling (FDM), developed by Stratasys. Process parameters such as raster angle, layer thickness, infill pattern and density, printing speed, and air gap influence the mechanical properties of the printed parts [7–9]. The properties of the parts are significantly influenced by the raster angle and layer thickness. These parameters govern the mesostructure of the printed part and therefore the properties of the part.

Furthermore, the build orientation of the model significantly influences the mechanical behavior of the printed part [10–13]. The effect of process parameters and build orientation results in the anisotropic nature of the part. The mechanical behavior of FDM printed parts resembles that of laminate structures [3, 14–17]. Such material behavior is mainly due to the orientation of fibers and the deposition of layers while printing the part. The printing direction, layer thickness, and orientation of the model influence the mechanical behavior of the printed parts [18–20]. The bonding between the layers as well as adjacent fibers governs the performance of the part [21], and the strength of bonding can also be affected by process parameters [22]. Pores in the microstructure of the printed parts were inherited from the printing process and such pores influence the mechanical properties of the parts. A real time detection of pores while printing parts using non-destructive techniques [22, 23] is useful for the evaluation their material properties and also to aid in certifying the parts.
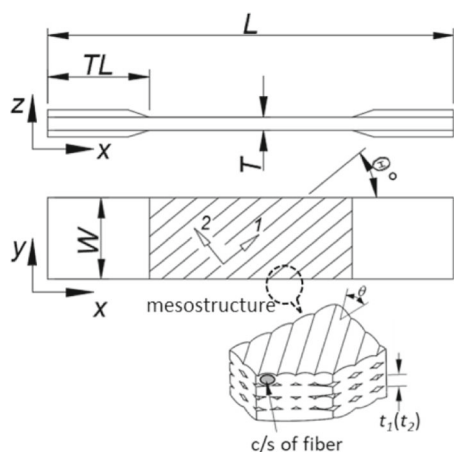
(a) *L*-Total length, *TL*- Tab length, *W*-Width, T-Thickness, *θ°* -Fiber direction to *x*-axis
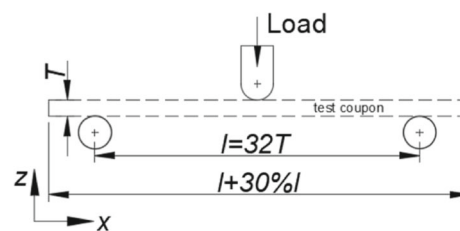
(b) *l*-Span distance, *l*+30%*l*- Total length, *T*-thickness, *W*-width

Fig. 2 Test coupons (a) tensile test (b) flexural test coupon

Table 1 Dimensions of the test coupons

Laminates	Layup No.	L	W	T	TL
Tensile test coupon dimensions, in mm					
Unidirectional	1 to 4	190	12.7	2.54	38
	5	127	25.4	2.54	19
Bidirectional	6 to 8	200	25.4	2.54	30
Flexural test coupon dimensions, in mm					
Bidirectional	9 to 11	$T = 3.17$, $W = 13$, $l = 32$ T, $L = l + 30\%l$			

The failure behavior of the printed parts is complex and is due to the anisotropic behavior of the material. The fracture development and the mechanical behavior of the printed composite laminates is addressed in [24, 25]. The performance of printed parts and analysis of their damage under fatigue loads has been investigated [26]. Failure behavior of composites subject to different loads can be characterized using micro computed tomography (μ-CT) as well as digital image correlation (DIC) [27, 28] The μ-CT and DIC can also help in identifying the damage mechanism of the parts. The presence of carbon fiber reinforcements in the polymer filament affects the mechanical failure behavior of the printed parts [29]. The failure behavior investigation of unidirectional printed parts is addressed in [30, 31]. Further exploration of the various mesostructural aspects of printed parts is needed to establish that the mechanical behavior of the printed parts is the same as that of the laminate structures.

In the present work, experimental test coupons with polymeric filament material were printed via FFF machine for tensile and bending tests. Parts with different raster orientations and two different layer thicknesses were printed to investigate the resulting mechanical behavior of the parts. We also examined the mechanical behavior of the printed test coupons under uniaxial tensile and bending loads. The influence of printing direction in each layer i.e., the effect of lamina lay-up on the mechanical behavior of the printed laminates subjected to loads was investigated. The mechanics of laminates was employed to characterize the mechanical behavior of printed parts. Failure analysis of the printed parts was then carried out using finite element method. Furthermore, a DIC setup was employed to characterize the failure behavior of the parts.

Methodology

In FFF, a polymeric filament material is melted in the extruder and then the molten material is extruded through the fine nozzle to deposit on the substrate. The three dimensional part is obtained by layer upon layer deposition of the material. The fabrication process of the method is shown in the Fig. 1. The parts printed via FFF resemble laminate structures and further the parts can be printed with different layer thicknesses (t) and fiber orientation ($\theta°$). Therefore, the printed parts also termed as printed laminates in the following sections. Further, the layers of a printed part are referred to as laminae and the extruded polymeric material is described as fibers, shown in Fig. 1. The fibers are extruded from a circular cross-section, but they take an elliptical shape after deposition on the

Table 2 Laminate lay-up and layer thickness used for printing laminate test coupons

Laminate	Lay-up No.	Raster angle ($\theta°$)	Layer thickness (t)	
			$t_1 = 0.317$	$t_2 = 0.158$
Unidirectional	1	0°	×	×
	2	30°	×	×
	3	45°	×	×
	4	60°	×	×
	5	90°	×	×
Bidirectional	6a	[0°/90°]$_{2S}$	×	−
	6b	[0°/90°]$_{4S}$	−	×
	7a	[45°/−45°]$_{2S}$	×	−
	7b	[45°/−45°]$_{4S}$	−	×
	8a	[(45°)$_2$/(−45°)$_2$]$_S$	×	−
	8b	[(45°)$_2$/(−45°)$_2$]$_{2S}$	−	×
Bidirectional	9a	[0°/90°/0°/90°/0°]$_S$	×	−
	9b	[0°/90°/0°/90°/0°]$_{2S}$	−	×
	10a	[45°/−45°/45°/−45°/45°]$_S$	×	−
	10b	[45°/−45°/45°/−45°/45°]$_{2S}$	−	×
	11a	[(45°)$_2$/(−45°)$_2$/45°]$_S$	×	−
	11b	[(45°)$_2$/(−45°)$_2$/45°]$_{2S}$	−	×
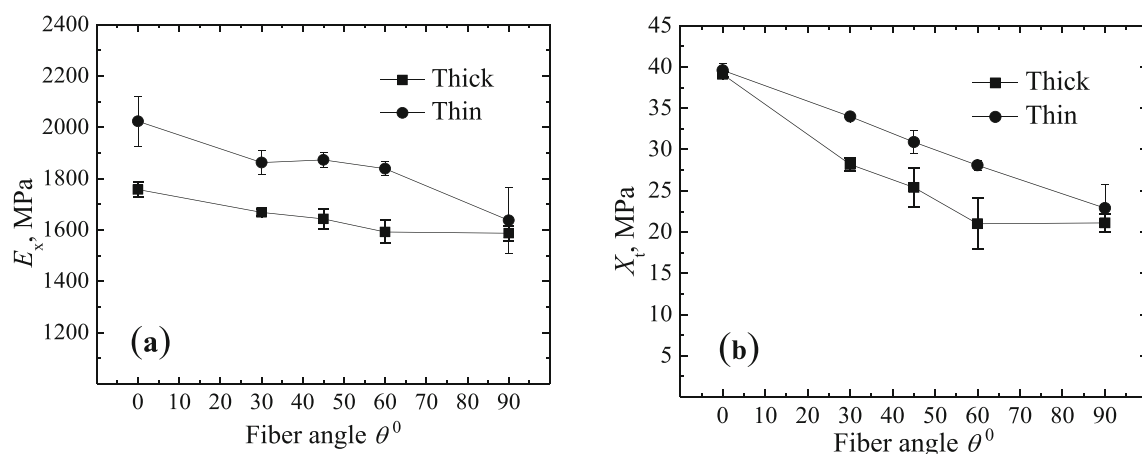
Fig. 3 Mechanical properties of unidirectional laminates: (*a*) $E_x - \theta°$ and (*b*) $X_t - \theta°$ for thick-layered (t_1) laminates, and thin-layered (t_2) laminates

substrate [32–34]. The size of the fibers is governed by the thickness of the layers defined for printing a part. For instance, if t is the layer thickness defined for printing and then, the size of deposited fibers equal to t as shown in the mesostructure of (Fig. 2(a)). The following section describes the mechanical test procedures and materials adopted for experimental investigation on printed laminates. Also, the process parameters employed for fabricating different type laminates are discussed.

Mechanical Testing

The parts were printed using commercially available isotropic thermoplastic material (ABS). The filament material spool was purchased from filament manufacturer 3DXTech (Byron Center, Michigan, USA) and the diameter of filament is 2.85 mm. Layer thickness and raster angle are two significant process parameters governing the mesostructure of the printed laminates. The raster angle defines the fiber orientation (angle) for the laminate lay-up, and the layer thickness represents the thickness of the lamina of the printed laminates and also the cross-sectional size of the fibers. Different types of unidirectional and bidirectional laminates are printed by varying these process parameters. The lamina lay-up in the printed bidirectional laminates is balanced and symmetric. Laminates of two different layer thicknesses are printed and the thickness of lamina (t_2) of thin layered laminate is half of the thickness of lamina (t_1) of thick layered laminate, However, the thickness of all layers within a laminate is the same. The mechanical behavior of the printed laminates under two different loads cases, uniaxial tensile and bending, were investigated. The test coupons were printed as per ASTM D3039 for tensile testing and ASTM D7264 for flexural testing. The printed parts behave as laminate structures, and therefore the ASTM test standards for laminate composites were adopted in the present work, and the mechanics of laminates were employed in experimental analyses.

The dimensions of the test coupons for the tensile and flexural cases are presented in Fig. 2 and Table 1. The laminate test coupons printed for mechanical testing using different lamina lay-ups and process parameters are presented in Table 2. The x, y, and z coordinates represent the global system for a laminate. Local coordinate system for a lamina is represented with 1, 2, and 3, where 1 denotes the fiber direction, and 2 and 3 are transverse to the orientation of the fibers, and this can be seen in (Fig. 2(a)).

For each test case, five coupons were printed. For instance, the lay-up 1 laminate can be of two different layer thicknesses (t_1 and t_2), resulting in a total of 10 coupons being printed for this case alone, as presented in Table 2. The raster angle represents the orientation of fibers in the layers of the laminate along the x-axis of the test coupon. This means that the fibers in unidirectional laminate lay-up 1 are oriented only along the axis of loading, and in the other cases the fibers are off-axis to loading. The difference in the bidirectional laminates of the same lay-up order is in the thickness of their layers. For example, the bidirectional laminate layup 6a and 6b have same layup order but of different layer thicknesses, it can be seen in the Table 2 that the layers of the laminate 6a are thicker than the laminate layup 6b. Three different layup types; cross ply $[0°/90°]_n$, angle ply $[45°/−45°]_n$, angle ply $[(45°)_2/(−45°)_2]_n$ bidirectional laminates were considered for investigation. The

Table 3 Mechanical properties of a lamina of the printed laminates

	Thick lamina (t_1)	Numerical [11], (t_1)	Thin lamina (t_2)
E_1, MPa	1757.7 ± 29.5	2025.1	2023.6 ± 96.8
E_2, MPa	1587.3 ± 28.7	1660.2	1637.6 ± 129.1
G_{12}, MPa	612.6 ± 25.1	674.3	744.7 ± 13.9
ν_{12}	0.35 ± 0.05	0.34	0.32 ± 0.06
X_t, MPa	39.1 ± 0.33	–	39.6 ± 0.8
Y_t, MPa	21.1 ± 1.1	–	22.9 ± 2.9
S, MPa	16.1 ± 2.5	–	21.3 ± 1.4

Table 4 Mechanical properties of cross-ply laminates under tensile loading

	Thick lamina (t_1)	Thin lamina (t_2)
E_x, MPa	1783.9 ± 2.7	1953.8 ± 55.8
E_x, MPa (CLT)	1673.0	1832.4
U_t, MPa	29.7 ± 0.7	35.7 ± 0.6
σ_{ply}, MPa (FE)	25.2	30.3
ε_t	0.0367 ± 0.0135	0.0498 ± 0.0004
ε_{ply} (FE)	0.0135	0.0143

Table 6 Mechanical properties of the angle-ply (lay-up 8) laminates under tensile loading

	Thick lamina (t_1)	Thin lamina (t_2)
E_x, MPa	1795.7 ± 1.3	1935.9 ± 1.7
E_x, MPa (CLT)	1645.6	1885.2
U_t, MPa	31.5 ± 0.3	34.9 ± 0.1
σ_{ply}, MPa (FE)	25.5	31.8
ε_t	0.0612 ± 0.0012	0.0839 ± 0.0059
ε_{ply} (FE)	0.0143	0.0158

other process parameters used for printing were as follows: an extruder temperature of 235 °C, a substrate temperature of 80 °C, a printing speed of 50 mm/s, 1 shell, an overlap between adjacent fibers of 15%, and an infill density of 100%. A total of 80 coupons were printed for tensile testing and 30 coupons for flexural testing on an Ultimaker printer. Laminate test coupons for lay-ups 1 to 8 were subjected to a uniaxial tensile load along x-axis (Fig. 2(a)), and lay-ups 9 to 11 were subjected to a transverse load (Fig. 2(b)).

The mesostructure of the printed laminates is mainly defined by the materials used for printing, the size of the fibers, the thickness of the layers, and the orientation of the fibers. These elements determine the mesostructure of the printed part and in turn govern the mechanical properties of the part. Therefore, a detailed investigation of different aspects of the mesostructure of the printed part can help to characterize the mechanical behavior of the parts using laminate mechanics. Test results reveal the mechanical properties of the printed laminates and also the behavior of the laminates under tensile and flexural loads. Furthermore, test results are useful for studying the influence of mesostructure on mechanical properties, which are in turn governed by the printing process. The elastic moduli of the stiffness matrix of the lamina can be calculated from the tensile test results and also its strength parameters. The flexural properties of the laminates and behavior can be found from the flexural test results. Finally, the results are useful for characterizing the mechanical behavior of the printed parts and also design and analysis of the printed parts using finite element method.

Results and Discussion

Tests were conducted on an MTS testing machine equipped with a 10 kN load cell for measuring load. The displacements of the test coupons during deformation were recorded using a laser extensometer. A digital image correlation setup (LaVision GmbH) was employed during tensile testing of certain coupons to measure strain. Tests were carried out at a quasi-static loading rate of 1 mm/min. Let us consider the tensile tests results of unidirectional and bidirectional printed laminates. The variation in the mechanical properties of thick-layered unidirectional printed laminates as well as thin-layered printed laminates is shown in Fig. 3. The x-axis of the graphs indicates the fiber orientation of the unidirectional laminates with respect to the x-axis of the laminate. The stiffness (E_x) and tensile strength (X_t) of the thin layered laminates is higher than that of thick layered unidirectional laminates. The laminates with fibers oriented along the loading axis have higher stiffness and strength than the laminates whose fibers are off-angle to the loading axis. Lay-up 1 laminates have higher stiffness and strength than lay-up 5 laminates, whose fibers are not oriented along the loading axis. This means that the printed parts will have directional properties and their fibers are the main load-taking members of the part.

The results for laminate lay-ups 1, 3, and 5 can be used to calculate the mechanical properties of the lamina. The layers of the printed parts behave as unidirectional fiber reinforced lamina. The elastic moduli and strength parameters of thick-

Table 5 Mechanical properties of the angle-ply (lay-up 7) laminates under tensile loading

	Thick lamina (t_1)	Thin lamina (t_2)
E_x, MPa	1790.7 ± 16.4	1911.1 ± 20.9
E_x, MPa (CLT)	1645.6	1885.2
U_t, MPa	28.0 ± 1.3	32.1 ± 0.7
σ_{ply}, MPa (FE)	25.5	31.8
ε_t	0.0435 ± 0.0049	0.0592 ± 0.0081
ε_{ply} (FE)	0.0143	0.0158

Table 7 Flexural properties of bidirectional laminates

	E^f_x, MPa	CLT E^f_x, MPa	U^f_x, MPa
Thick layer (t_1)			
Lay-up 9a	1818.1 ± 49.5	1698.2	41.4 ± 0.7
Lay-up 10a	1813.9 ± 17.8	1645.5	41.1 ± 1.1
Lay-up 11a	1965.6 ± 18.0	1645.1	48.1 ± 0.4
Thin layer (t_2)			
Lay-up 9b	2382.7 ± 74.0	1875.6	50.5 ± 1.4
Lay-up 10b	2324.5 ± 34.3	1884.7	52.7 ± 0.8
Lay-up 11b	2426.6 ± 3.50	1884.4	57.5 ± 0.4
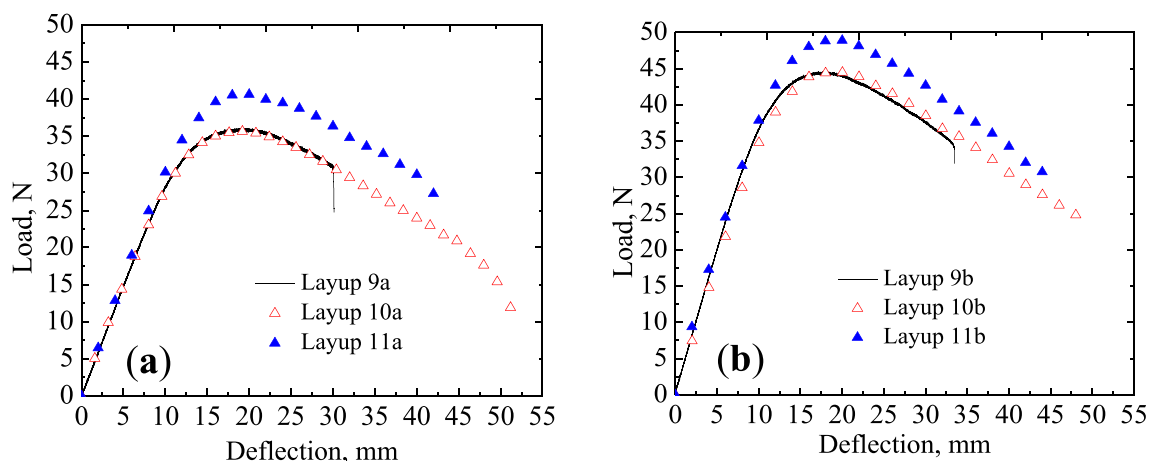
Fig. 4 Load versus deflection curves of (*a*) thick-layered laminates and (*b*) thin-layered laminates

layered laminates and also, thin-layered laminates are presented in Table 3. Strain data for the calculation of Poisson's ratio were measured using a digital image correlation setup. The strength parameters of the lamina, denoted X_t and Y_t, are the tensile strengths longitudinally and transversely, respectively, and S is the in-plane shear strength. The properties E_1, ν_{12} and X_t were calculated from results of lay-up 1, and E_2 and Y_t were obtained from the results of lay-up 5. The results of lay-up 3 laminate were used for the calculation of G_{12} and S [35]. The elastic moduli of thick layered laminate were validated with existing numerical results [11] and the numerical results were obtained by replicating the mesostructure of a printed part in a finite element model used to calculate the elastic moduli via the homogenization technique. The discrepancy in the results is due to that the bonding between adjacent fibers is assumed perfect in that numerical analysis, but it is not true in the actual printed parts. These mechanical properties are useful for the stress analysis of the printed parts using the finite element method.

Next, bidirectional laminates with three different lay-up orders were tested: cross-ply laminate (lay-up 6) and angle-ply laminates (lay-ups 7 and 8). The laminates with lay-ups

6a, 7a, and 8a are thick-layered laminates and those with lay-ups 6b, 7b, and 8b are thin-layered laminates. The tensile properties of the bidirectional laminates are presented in Table 4 for cross-ply laminates, Table 5 for angle-ply laminates of lay-up 7, and Table 6 for angle-ply laminates of lay-up 8. The tensile modulus (E_x) of the laminates was validated using the classical laminate theory (CLT), see Appendix A, and results were in good agreement. The calculations for tensile modulus of a laminate based on CLT employ the elastic moduli of a lamina available in Table 3. Also, ultimate tensile strength (U_t) and the strain to failure (ε_t) are presented in Tables 4, 5 and 6. The difference in the results of the thick- and thin- layered bidirectional laminates is due to change in the aspects of their mesostructure. Further, tensile testing of the laminates was modeled with 2D PCOMPG finite elements (FE) in Hyperworks, Altair and then simulated for the failure analysis. The first ply failure theory, Tsai-Hill failure criterion, was used for failure analysis. The principal stress (σ_{ply}) of the first ply failure and the corresponding elastic ply strain (ε_{ply}) of the laminates are also reported in the Tables 4, 5 and 6. The tensile modulus obtained using CLT and the ply failure stress from FE analysis are less than the corresponding experimental
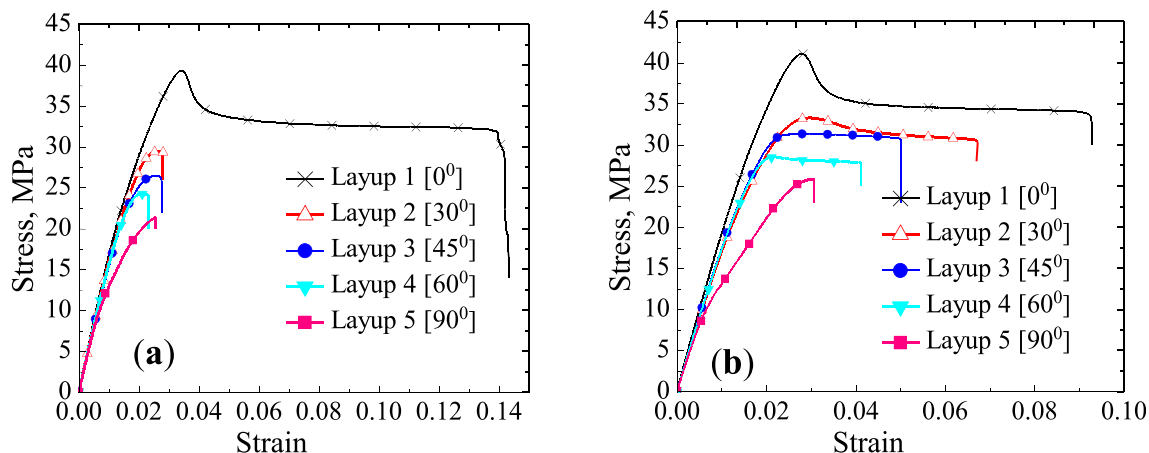
Fig. 5 Stress–strain curves of unidirectional laminates for (*a*) thick layered laminates, and (*b*) for thin layered laminates
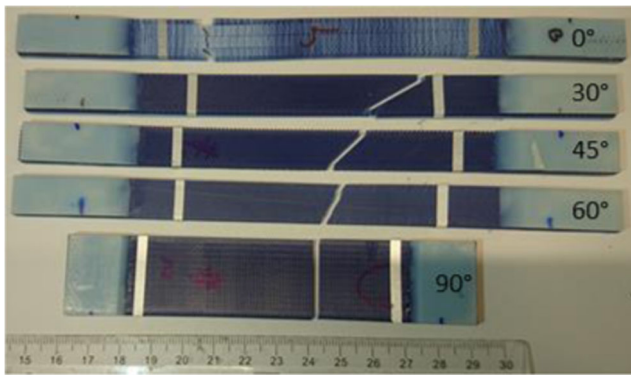
Fig. 6 Fracture lines of the printed laminates subject to uniaxial tensile loading

results of the laminates. This difference in the results is mainly due to the elastic moduli (Table 3) that were used in the CLT and failure theory. The elastic moduli in Table 3 were calculated from the tensile test results of the unidirectional laminates. Such test results of unidirectional laminates were significantly influenced by bonding at the interface of layers when compared to bidirectional laminates [22, 33]. Influence of bonding at interface of the layers of unidirectional and the bidirectional laminates on their properties is discussed in detail in later part of the section.

Flexural Results

Three-point bending tests were conducted on cross-ply and angle-ply printed laminates. The lay-up order of the laminates for bending tests is presented in Table 2. The laminates with lay-up 9a, 10a, and 11a are thick-layered laminates, and those with lay-up 9b, 10b, and 11b are thin-layered laminates. Flexural properties of the laminates are presented in Table 7. The flexural stiffness of the laminates calculated from the test results was validated with analytical stiffness. The analytical calculations for the stiffness of the laminates are based on classical laminate theory, see Appendix A. The elastic moduli of the lamina from Table 3 were employed for calculating flexural stiffness of the laminate using classical laminate theory. Experimental and analytical stiffness values of the

laminates were in good agreement. The difference between the experimental and analytical results for the printed laminates indicates that the laminate theory under predicts flexural stiffness. This inaccuracy due to the elastic moduli of the lamina from Table 3 were employed in the calculation of stiffness using CLT. The flexural stiffness (E^f_x) and flexural strength (U^f_x) of thin-layered laminate lay-up types is higher than that of thick-layered laminate. Load versus deflection curves for the laminates are shown in Fig. 4. The curves illustrate that the angle-ply laminates undergo more deflection than the cross-ply laminates with the same layer thickness.

Next, the effect of lamina lay-up and layer thickness on the failure behavior of the laminates under tensile and flexural loads is discussed. The stress–strain curves of the unidirectional laminates made of two different layer thicknesses are shown in Fig. 5. Two types of failure modes, namely fiber breakage and fiber debonding, were seen in the laminates under these loads. Failure modes of the unidirectional laminates can be seen in Fig. 6. The lay-up 1 laminates saw these two failure modes, and the other unidirectional laminate lay-ups saw only the debonding failure mode under tensile loads. This difference is owing to the orientation of the fibers in the other unidirectional laminates being off-axis to loading, and therefore a significant amount of load was shared by the interface of the fibers in the laminate layer. The interface has a lower bonding strength than the fiber and therefore, the interface experiences early failure before breakage of the fibers. This can be observed in the stress–strain curves that the laminates with layup 2 to 5 subjected to early failure compared to layup 1 laminate. Therefore, the properties of the lamina obtained from these tests are not very accurate because of significant influence of the bonding in such laminates on contrast to the bidirectional laminates. The mesostructure of the unidirectional and bidirectional laminates, captured using microscope BX41M-LED from Olympus Corporation, are shown in Fig. 7.

The mesostructure of the printed part will contain voids inherited from the printing process. The difference in the results for thick-layered laminate and thin-layered laminate lay-ups is due to variation in the size of the voids in the laminates'

Fig. 7 Mesostructure of printed laminates, (*a*) unidirectional laminate, (*b*) bidirectional cross-ply laminate
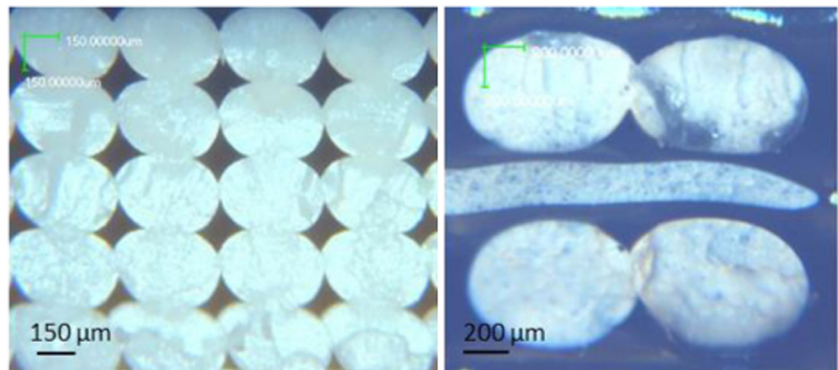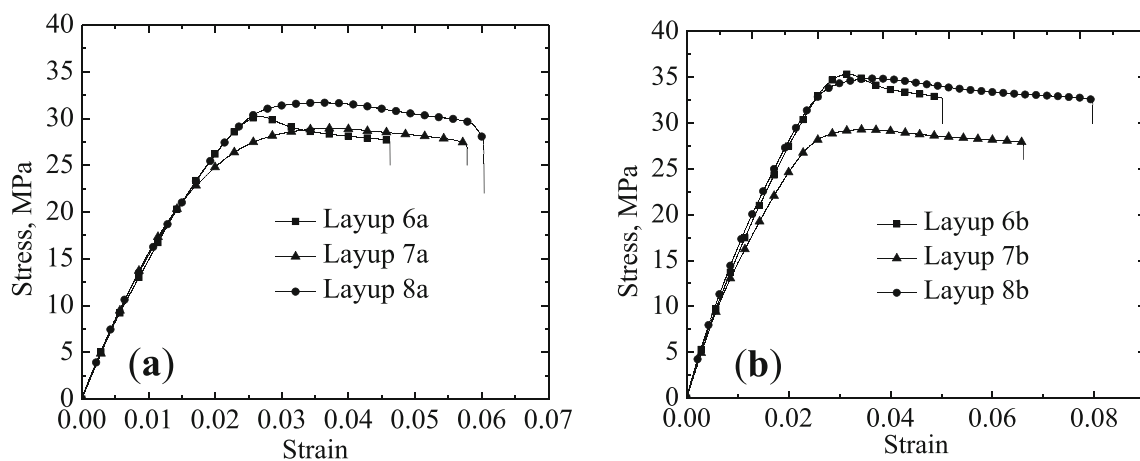
Fig. 8 Stress–strain curves of bidirectional laminates: for (*a*) thick-layered laminates and (*b*) thin-layered laminates

mesostructure. The size of the voids in the thin-layered laminate is smaller than those in the thick-layered laminate, and the bonding is stronger between the fibers for laminates with a smaller void size and density. Void size affects the mechanical behavior of the unidirectional laminates more than that of the bidirectional laminates. This effect could explain the difference in the stress–strain curves of the thick- and thin-layered unidirectional laminates as well as bidirectional laminates. The stress–strain curves of the bidirectional laminates are shown in Fig. 8. The size of the voids can be minimized by lowering layer thickness and increasing overlap between the fibers. The variation in the results for different laminates is mainly due to changes in various aspects of their

mesostructure, including size of the fibers, thickness of layers, and orientation of the fibers.

The strain distribution just before propagation of the crack in the thick-layered laminates subjected to tensile loading is shown in Fig. 9. The failure strain of the thick layered laminates is lower than that of the thin layered laminates. Also, failure strain is higher for angle-ply laminates than for cross-ply laminates. The angle-ply bidirectional laminates experienced fiber breakage only, whereas the cross-ply laminates saw both failure modes. This is means that the interaction of fibers between the adjacent layers of the laminate played a role in sharing the applied load. The thin-layered laminates are stronger and stiffer than the thick-layered laminates. This is
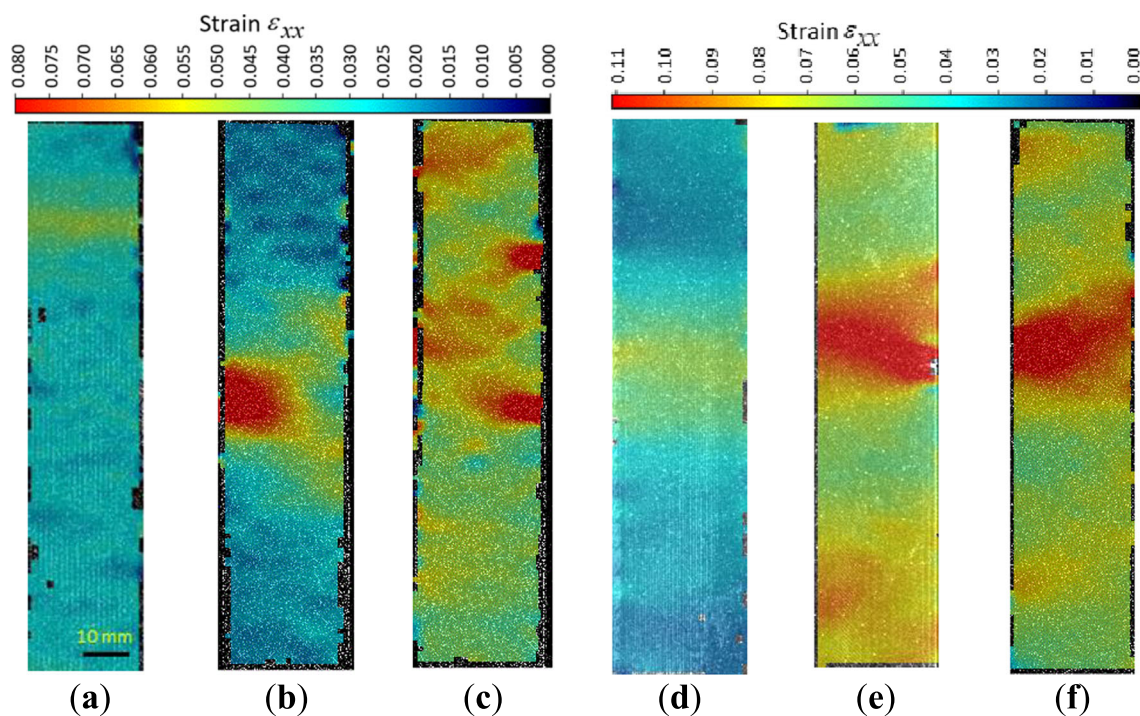
Fig. 9 Strain distribution in the laminates during tensile testing. Thick layered laminates: (*a*) lay-up 6a, (*b*) lay-up 7a, and (*c*) lay-up 8a. Thin layered laminates: (*d*) lay-up 6b, (*e*) lay-up 7b, and (*f*) lay-up 8b

because of bonding between the fibers as well as between the layers is stronger in thin-layered laminates than in thick-layered laminates.

The first ply failure criteria can be adopted for preliminary design and analysis of the printed parts. More importantly, the properties useful in the design and failure analysis of the parts need careful evaluation, since the properties such as elastic moduli and strength parameters are calculated from experimental results of unidirectional printed laminates. Following this work, a detailed damage analysis of the printed laminates can be carried out using computational methods. The computational multiscale models [36] can account for the different mesostructural aspects of the printed parts for material modeling and also damage modeling of printed laminates. The computational multiscale models for 3D printed laminates can allow for effective design of the mesostructure and also stress analysis of the printed structures.

Conclusions

In this work, the role of aspects of the mesostructure on the overall mechanical properties of 3D printed parts was investigated experimentally. In particular, we studied influence of orientation of fibers, layer thickness and lamina layup on the properties of the printed parts. The aspects of the mesostructure are defined by process parameters, and in turn these parameters govern the mechanical behavior of the printed parts. Tensile tests were conducted on unidirectional laminates of different layer thicknesses test coupons. Then, in-plane elastic moduli and the strength parameters of a lamina of the printed parts are calculated using laminate mechanics from the tensile test results of unidirectional laminates. These properties of lamina are useful in the finite element analysis of the printed parts. Then tensile and flexural tests were conducted on three different lamina layup bidirectional laminates to characterize the mechanical behavior of the printed parts. The classical laminate theory was employed for the validating the experimental results of bidirectional laminates subject to tensile and bending loads. Analytical results are in good agreement with experiment work for bidirectional laminates. Further, FE analysis was carried out for failure behavior of the laminates. The validation of experimental results by analytical and FE findings reveals that the laminate mechanics works better for characterizing the mechanical behavior of printed parts. The influence of lay-up and layer thickness on the tensile properties of unidirectional laminates is higher in contrast to bidirectional laminates. Furthermore, the effect of lamina lay-up and layer thickness on the flexural properties of bidirectional laminates is relatively higher than their effect on tensile properties. The bidirectional laminates subjected to tensile and flexural loads exhibit higher plasticity and followed by ductile failure. Preliminary design and analysis of the parts for 3D printing via FFF can be done using the first ply failure theory. Finally, insights gained from relation of mesostructure–properties–performance of printed parts in the present study will help for effective design and analysis of structural parts for 3D printing.

Appendix A

Classical Laminate Theory

The constitutive relation of a lamina is written as

$$
\begin{Bmatrix} \sigma_{11} \\ \sigma_{22} \\ \tau_{12} \end{Bmatrix} = \begin{bmatrix} Q_{11} & Q_{12} & 0 \\ Q_{12} & Q_{22} & 0 \\ 0 & 0 & Q_{66} \end{bmatrix} \begin{Bmatrix} \varepsilon_{11} \\ \varepsilon_{22} \\ \gamma_{12} \end{Bmatrix} \text{ in short } \{\sigma\} = [Q]\{\varepsilon\}
$$

(1)

where

$$
Q_{11} = \frac{E_1}{1 - \nu_{12}\nu_{21}}, Q_{12} = \frac{\nu_{12}E_1}{1 - \nu_{12}\nu_{21}}, Q_{22} = \frac{E_2}{1 - \nu_{12}\nu_{21}}, Q_{66} = G_{12}
$$

(2)

Strains of the laminate is written as

$$
\begin{Bmatrix} \varepsilon_{xx} \\ \varepsilon_{yy} \\ \gamma_{xy} \end{Bmatrix} = \begin{Bmatrix} \varepsilon_{xx}^0 \\ \varepsilon_{yy}^0 \\ \gamma_{xy}^0 \end{Bmatrix} + z \begin{Bmatrix} k_{xx} \\ k_{yy} \\ k_{xy} \end{Bmatrix}, \text{ in short } \{\varepsilon\} = \{\varepsilon^0\} + z\{k\} \quad (3)
$$

where $\{\varepsilon^0\}$ are in-plane strains; $\{k\}$ are curvatures of the laminate; z is distance from mid plane in the thickness direction. The constitutive matrix for a lamina in global coordinate system is given as

$$
\{\sigma\} = \left[\overline{Q}\right]\{\varepsilon\}
$$

(4)

where $\overline{Q}_{ij}$ is written as $\left[\overline{Q}\right] = [T]^{-1}[Q][T]^{-T}$ and $[T]$ is a transformation matrix. The resultant force and moment per unit width for a laminate with N number of layers are expressed as

$$
\{N\} = \sum_{k=1}^{N} \int_{h_k}^{h_{k+1}} \{\sigma\} \, dz
$$

(5)

$$
\{M\} = \sum_{k=1}^{N} \int_{h_k}^{h_{k+1}} \{\sigma\} z \, dz
$$

(6)

Using (equation (3), (4)), and (equation (5), (6)) become

$$
\{N\} = [A]\{\varepsilon^0\} + [B]\{k\}
$$

(7)

$$
\{M\} = [B]\{\varepsilon^0\} + [D]\{k\}
$$

(8)

where $[A] = \sum\limits_{k=1}^{N} \left[\overline{Q}\right]_k (z_k - z_{k-1})$, $[B] = \frac{1}{2} \sum\limits_{k=1}^{N} \left[\overline{Q}\right]_k \left(z_k^2 - z_{k-1}^2\right)$, $[D] = \frac{1}{3} \sum\limits_{k=1}^{N} \left[\overline{Q}\right]_k \left(z_k^3 - z_{k-1}^3\right)$.

The $[A]$, $[B]$ and $[D]$ are stiffness matrices for the laminate. The $[B] = [0]$ for a symmetric laminate. The mid-plane strains and curvatures can be calculated from (equation (7), (8)), once we know the normal force and moment acting on a lamina. Strains for a symmetric laminate subjected to only in-plane forces are given from (equation (7)) as

$$\begin{Bmatrix} \varepsilon_{xx}^0 \\ \varepsilon_{yy}^0 \\ \gamma_{xy}^0 \end{Bmatrix} = [A]^{-1} \begin{Bmatrix} N_{xx} \\ N_{yy} \\ N_{xy} \end{Bmatrix} \qquad (9)$$

Strains for a symmetric laminate subjected to only transverse loads are given from (equation (8)) as

$$\begin{Bmatrix} k_{xx} \\ k_{yy} \\ k_{xy} \end{Bmatrix} = [D]^{-1} \begin{Bmatrix} M_{xx} \\ M_{yy} \\ M_{xy} \end{Bmatrix} \qquad (10)$$

Uniaxial tensile loading along x-axis: In the uniaxial tensile test, the load is applied in the x direction and for laminate thickness h, $N_{xx} = h\sigma_{xx}$ $N_{yy} = 0$ and $N_{xy} = 0$. The stress-strain relation for uniaxial tensile test is $\sigma_{xx} = E_{xx}\varepsilon_{xx}^0$, using the relation (equation (9)), the modulus of elasticity along the x direction of the laminate is calculated as follows

$$E_{xx} = \frac{1}{\left[A^{-1}\right]_{11} h} \qquad (11)$$

Flexural loads: In the 3-point bending test, the load is applied in the z direction and for laminate thickness h, $M_{xx} \neq 0$, $M_{yy} = 0$ and $M_{xy} = 0$. The relationship between flexural stress and stiffness is written as $E_x^f = \sigma_{xx}^f / \varepsilon_{xx}^f$, using the (equation (10)), the flexural modulus of elasticity of the laminate along the x direction is given as follows

$$E_x^f = \frac{12}{\left[D^{-1}\right]_{11} h^3} \qquad (12)$$

The elastic moduli such as E_1, E_2, G_{12}, ν_{12} of the lamina found from the experimental tensile test results are used for the calculation of matrices $[A]$, $[B]$ and $[D]$. Then, E_{xx} and E_x^f of the laminate can be calculated using (equation (11), (12)), respectively. More details about the laminate theory available in [35].

Tsai-Hill Failure Criterion

The failure criterion for a planar stress is written as

$$\frac{\sigma_1^2}{X^2} - \frac{\sigma_1 \sigma_2}{X^2} + \frac{\sigma_2^2}{Y^2} + \frac{\tau_{12}^2}{S^2} = 1 \qquad (13)$$

The lamina properties available in Table 3 are useful in the failure analysis of the printed laminates. The nonlinear quasi-static finite element failure analysis of the laminates was done in Hyperworks. The first ply failure stresses and corresponding strains are reported in the results when the laminate just met the failure criterion. More details about the nonlinear quasi static analysis and finite element modeling of composites laminates can be found in the Hyperworks manual.

References

1. Gao W, Zhang Y, Ramanujan D et al (2015) The status, challenges, and future of additive manufacturing in engineering. Comput Des 69:65–89
2. Quan Z, Wu A, Keefe M, Qin X, Yu J, Suhr J, Byun JH, Kim BS, Chou TW (2015) Additive manufacturing of multi-directional preforms for composites: opportunities and challenges. Mater Today 1;18(9):503–12
3. Ahn SH, Montero M, Odell D, Roundy S, Wright PK (2002) Anisotropic material properties of fused deposition modeling ABS. Rapid Prototyp J 8(4):248–257
4. Jiang D, Smith DE (2017) Anisotropic mechanical properties of oriented carbon fiber filled polymer composites produced with fused filament fabrication. Addit Manuf 18:84–94
5. Guessasma S, Belhabib S, Nouri H, Hassana OB (2016) Anisotropic damage inferred to 3D printed polymers using fused deposition modelling and subject to severe compression. Eur Polym J 85:324–340
6. Torrado AR, Roberson DA (2016) Failure analysis and anisotropy evaluation of 3D printed tensile test specimens of different geometries and print raster patterns. J Fail Anal Prev 16(1):154–164
7. Wu W, Geng P, Li G, Zhao D, Zhang H, Zhao J (2015) Influence of layer thickness and raster angle on the mechanical properties of 3D-printed PEEK and a comparative mechanical study between PEEK and ABS. Materials. 8(9):5834–5846
8. Popescu D, Zapciu A, Amza C, Baciu F, Marinescu R (2018) FDM process parameters influence over the mechanical properties of polymer specimens: a review. Polym Test 69:157–166
9. Cantrell JT, Rohde S, Damiani D et al (2017) Experimental characterization of the mechanical properties of 3D-printed ABS and polycarbonate parts. Rapid Prototyp J 23(4):811–824
10. Zaldivar RJ, Witkin DB, McLouth T, Patel DN, Schmitt K, Nokes JP (2017) Influence of processing and orientation print effects on the mechanical and thermal behavior of 3D-printed ULTEM® 9085 material. Addit. Manuf. 13:71–80
11. Somireddy M, Czekanski A, Singh CV (2018) Development of constitutive material model of 3D printed structure via FDM. Mater Today Commun 15:143–152
12. Türk DA, Brenni F, Zogg M, Meboldt M (2017) Mechanical characterization of 3D printed polymers for fiber reinforced polymers processing. Mater Des 118:256–265
13. Chacón JM, Caminero MA, García-Plaza E, Núñez PJ (2017) Additive manufacturing of PLA structures using fused deposition modelling: effect of process parameters on mechanical properties and their optimal selection. Mater Des 124:143–157
14. Kulkarni P, Dutta D (1999) Deposition strategies and resulting part stiffnesses in fused deposition modeling. J Manuf Sci Eng 121(1):93–103
15. Casavola C, Cazzato A, Moramarco V, Pappalettere C (2016) Orthotropic mechanical properties of fused deposition modelling parts described by classical laminate theory. Mater Des 90:453–458

16. Somireddy M, Czekanski A (2017) Mechanical characterization of additively manufactured parts by FE modeling of mesostructure. J Manuf Mater Process 1(2):18

17. Domingo-Espin M, Puigoriol-Forcada JM, Garcia-Granada AA et al (2015) Mechanical property characterization and simulation of fused deposition modeling Polycarabonate parts. Mater Des 83: 670–677

18. Arbeiter F, Spoerk M, Wiener J, Gosch A, Pinter G (2018) Fracture mechanical characterization and lifetime estimation of near-homogeneous components produced by fused filament fabrication. Polym Test 66:105–113

19. Spackman CC, Frank CR, Picha KC, Samuel J (2016) 3D printing of fiber-reinforced soft composites: process study and material char-acterization. J Manuf Process 23:296–305

20. Rankouhi B, Javadpour S, Delfanian F, Letcher T (2016) Failure analysis and mechanical characterization of 3D printed ABS with respect to layer thickness and orientation. J Fail Anal Prev 16(3): 467–481

21. Aliheidari N, Tripuraneni R, Ameli A, Nadimpalli S (2017) Fracture resistance measurement of fused deposition modeling 3D printed polymers. Polym Test 60:94–101

22. Holzmond O, Li X (2017) In situ real time defect detection of 3D printed parts. Addit Manuf 17:135–142

23. Bartlett JL, Heim FM, Murty YV, Li X (2018) In situ defect detec-tion in selective laser melting via full-field infrared thermography. Addit Manuf. 24:595–605

24. Goh GD, Dikshit V, Nagalingam AP et al (2018) Characterization of mechanical properties and fracture mode of additively manufactured carbon fiber and glass fiber reinforced thermoplas-tics. Mater Des 137:79–89

25. Ferreira RTL, Amatte IC, Dutra TA, Bürger D (2017) Experimental characterization and micrography of 3D printed PLA and PLA re-inforced with short carbon fibers. Compos Part B Eng 124:88–100

26. Ziemian CW, Ziemian RD, Haile KV (2016) Characterization of stiffness degradation caused by fatigue damage of additive manufactured parts. Mater Des 109:209–218

27. Croom BP, Xu P, Lahoda EJ et al (2017) Quantifying the three-dimensional damage and stress redistribution mechanisms of braid-ed SiC/SiC composites by in situ volumetric digital image correla-tion. Scr Mater 130:238–241

28. Croom B, Wang WM, Li J, Li X (2016) Unveiling 3D deformations in polymer composites by coupled micro x-ray computed tomogra-phy and volumetric digital image correlation. Exp Mech 56:999–1016

29. Zhang W, Cotton C, Sun J, Heider D, Gu B, Sun B, Chou TW (2018) Interfacial bonding strength of short carbon fiber/acryloni-trile-butadiene-styrene composites fabricated by fused deposition modeling. Compos. Part B Eng. 137:51–59

30. Song Y, Li Y, Song W et al (2017) Measurements of the mechanical response of unidirectional 3D-printed PLA. Mater Des 123:154–164

31. Alaimo G, Marconi S, Costato L, Auricchio F (2017) Influence of meso-structure and chemical composition on FDM 3D-printed parts. Compos Part B Eng 113:371–380

32. Islam MS, Prabhakar P (2017) Interlaminar strengthening of mul-tidirectional laminates using polymer additive manufacturing. Mater Des 133:332–339

33. Tekinalp HL, Kunc V, Velez-Garcia GM et al (2014) Highly orient-ed carbon fiber-polymer composites via additive manufacturing. Compos Sci Technol 105:144–150

34. Koch C, Van Hulle L, Rudolph N (2017) Investigation of mechan-ical anisotropy of the fused filament fabrication process via custom-ized tool path generation. Addit Manuf. 16:138–145

35. Jones RM (1999) Mechanics of composite materials. Taylor & Francis, Philadelphia

36. Talreja R, Singh CV (2012) Damage and failure of composite ma-terials. Cambridge University Press, Cambridge